Identification of a brainstem locus that inhibits tumor necrosis factor

Adam M. Kressel[a,b,c], Tea Tsaava[a], Yaakov A. Levine[d], Eric H. Chang[a], Meghan E. Addorisio[a], Qing Chang[a], Barry J. Burbach[e], Daniela Carnevale[f,g], Giuseppe Lembo[f,g], Anthony M. Zador[e], Ulf Andersson[h], Valentin A. Pavlov[a,b,i,1], Sangeeta S. Chavan[a,b,i,2,1], and Kevin J. Tracey[a,b,i,2,1]

[a]Institute of Bioelectronic Medicine, The Feinstein Institutes for Medical Research, Northwell Health, Manhasset, NY 11030; [b]The Elmezzi Graduate School of Molecular Medicine, Manhasset, NY 11030; [c]Department of Surgery, North Shore University Hospital, Northwell Health, Manhasset, NY 11030; [d]Setpoint Medical, Valencia, CA 91355; [e]Cold Spring Harbor Laboratory, Cold Spring Harbor, NY 11724; [f]Department of Angiocardioneurology and Translational Medicine, IRCCS Neuromed, 86077 Pozzilli, IS, Italy; [g]Department of Molecular Medicine, Sapienza University of Rome, 00161 Rome, Italy; [h]Department of Women's and Children's Health, Karolinska Institute, Karolinska University Hospital, 17176 Stockholm, Sweden; and [i]Department of Molecular Medicine, Donald and Barbara Zucker School of Medicine at Hofstra/Northwell Health, Hempstead, NY 11549

Edited by Lawrence Steinman, Stanford University School of Medicine, Stanford, CA, and approved September 4, 2020 (received for review April 29, 2020)

In the brain, compact clusters of neuron cell bodies, termed nuclei, are essential for maintaining parameters of host physiology within a narrow range optimal for health. Neurons residing in the brainstem dorsal motor nucleus (DMN) project in the vagus nerve to communicate with the lungs, liver, gastrointestinal tract, and other organs. Vagus nerve-mediated reflexes also control immune system responses to infection and injury by inhibiting the production of tumor necrosis factor (TNF) and other cytokines in the spleen, although the function of DMN neurons in regulating TNF release is not known. Here, optogenetics and functional mapping reveal cholinergic neurons in the DMN, which project to the celiac-superior mesenteric ganglia, significantly increase splenic nerve activity and inhibit TNF production. Efferent vagus nerve fibers terminating in the celiac-superior mesenteric ganglia form varicose-like structures surrounding individual nerve cell bodies innervating the spleen. Selective optogenetic activation of DMN cholinergic neurons or electrical activation of the cervical vagus nerve evokes action potentials in the splenic nerve. Pharmacological blockade and surgical transection of the vagus nerve inhibit vagus nerve-evoked splenic nerve responses. These results indicate that cholinergic neurons residing in the brainstem DMN control TNF production, revealing a role for brainstem coordination of immunity.

vagus nerve | dorsal motor nucleus | inflammatory reflex | cytokines | TNF

In the evolutionary history of mammals, infection and injury have been the principal threats to the survival of species. The mammalian nervous system, comprising sensory, voluntary motor, and involuntary motor divisions, evolved to coordinate the mammalian physiological responses to internal and external environmental threat. Although it accounts for <3% of brain mass, the brainstem is crucial for regulating heart rate, blood pressure, respiration, swallowing, consciousness, and other fundamental physiological events. Clusters of neuron cell bodies, termed nuclei, in the brainstem are the origin of cranial nerves which transmit action potentials controlling organ function. Using stimulating electrodes in specific brainstem nuclei, it is possible to map the spatial organization of neurons which regulate precise cellular responses in organs. For example, stimulation of the dorsal motor nucleus (DMN) of the vagus in the brainstem medulla elicits the production of gastrointestinal peristalsis and gastric acid, insulin, and glucagon secretion (1–3). It also decreases mean arterial blood pressure, and increases left and right ventricular end diastolic pressure (4). Neuronal cell bodies residing in the DMN and nucleus ambiguus project axons within the vagus nerve, the longest nerve in the body, which innervates and coordinates organ responses to threat (5–8).

Injury and infection stimulate white blood cells in the immune system to produce cytokines and other signaling molecules. One cytokine, tumor necrosis factor (TNF), is a pivotal inflammatory mediator because its overproduction can be lethal, and its insufficient production can enhance the risk of infection (9–12). We and others found a critical role for the vagus nerve in controlling TNF production during injury and infection (13–16) which we termed the inflammatory reflex (17–20). Action potentials in the vagus nerve terminate in the celiac-superior mesenteric ganglion complex, the origin of the adrenergic splenic nerve (21–23). When the vagus nerve is electrically stimulated, norepinephrine released in the spleen stimulates a subset of T cells defined by expression of choline acetyltransferase, the enzyme that catalyzes the biosynthesis of acetylcholine (24). Acetylcholine signals through α7 nicotinic acetylcholine receptors (α7nAChR) expressed on red pulp and marginal zone macrophages to inhibit TNF production (25). Intracellular mechanisms downstream of α7nAChR activate the Janus kinase (JAK)2–signal transducer and activator of transcription (STAT)3 pathway, sequester Nuclear Factor-kB (NF-κB), and inhibit activation of the inflammasome (16, 18, 26, 27).

Significance

Electronic devices that stimulate electrical activity in the vagus nerve are being studied for clinical use in rheumatoid arthritis, inflammatory bowel disease, and other inflammatory syndromes because vagus nerve signals inhibit inflammation and cytokine production. A vagus nerve mechanism, termed the inflammatory reflex, has been widely studied, but the origin and functional neuroanatomy of vagus nerve fibers controlling inflammation were previously unknown. Here we reveal cholinergic neurons in the brainstem dorsal motor nucleus (DMN) of the vagus projecting to the celiac-superior mesenteric ganglia and transmitting cytokine-inhibiting signals to the splenic nerve. By combining optogenetics, anatomical and functional mapping, and measurement of TNF production, our data show the DMN is an important brainstem locus controlling anti-inflammatory signals in the inflammatory reflex.

Author contributions: A.M.K., Y.A.L., V.A.P., S.S.C., and K.J.T. designed research; A.M.K., T.T., Y.A.L., M.E.A., and Q.C. performed research; B.J.B., D.C., G.L., and A.M.Z. contributed new reagents/analytic tools; A.M.K., Y.A.L., E.H.C., V.A.P., S.S.C., and K.J.T. analyzed data; and A.M.K., Y.A.L., E.H.C., U.A., V.A.P., S.S.C., and K.J.T. wrote the paper.

Competing interest statement: A.M.K., V.A.P., S.S.C. and K.J.T. have filed a patent application relevant to this work and have assigned their rights to the Feinstein Institutes for Medical Research. Y.A.L. is an employee of SetPoint Medical.

This article is a PNAS Direct Submission.

[1]To whom correspondence may be addressed. Email: schavan@northwell.edu, vpavlov@northwell.edu, or kjtracey@northwell.edu.

[2]S.S.C. and K.J.T. contributed equally to this work.

This article contains supporting information online at https://www.pnas.org/lookup/suppl/doi:10.1073/pnas.2008213117/-/DCSupplemental.

First published November 9, 2020.

Experimentally, the inflammatory reflex can be studied using specific vagus nerve or splenic nerve-stimulating devices (13, 21, 28–32). Clinical studies of stimulating the inflammatory reflex by implanting a vagus nerve-stimulating device in patients with rheumatoid arthritis or Crohn's disease revealed significantly decreased TNF production and improved clinical outcomes (33–35).

Although it is possible to experimentally and clinically stimulate the vagus nerve to inhibit TNF production, it was previously unknown whether neurons residing in brainstem nuclei control the production of TNF production in the spleen. Using optogenetics and functional mapping, here we show that DMN cholinergic neurons project to the celiac-superior mesenteric ganglia to significantly increase splenic nerve activity and inhibit TNF production.

Results and Discussion

Selective Activation of DMN Cholinergic Neurons Inhibits TNF Production during Endotoxemia. We used optogenetic approaches to study the role of cholinergic neurons originating in the DMN regulating TNF production. Channelrhodopsins are cation channels that activate upon illumination by specific wavelengths of light (36). To selectively target brainstem DMN cholinergic neurons, we utilized mice expressing channelrhodopsin-2 (ChR2) coupled to an enhanced yellow fluorescent protein (ChR2-eYFP) directed by choline acetyl transferase (ChAT) promoter. ChAT expression defines the presence of cholinergic neurons in the central and peripheral nervous systems (37–39). Immunofluorescent staining of brain slices showed colocalization of ChAT-expressing cholinergic neurons and ChR2-eYFP in the brainstem DMN of ChAT-ChR2-eYFP mice (Fig. 1 *A–D*). The left DMN in ChAT-ChR2-eYFP mice was targeted and identified under stereotactic guidance (*SI Appendix*, Fig. S1), and cholinergic neurons in the DMN were selectively stimulated via a fiberoptic cannula. In agreement with our recent study demonstrating the anti-inflammatory effects of vagus nerve stimulation (VNS) performed 24h prior to endotoxin administration and to avoid the confounding effects of anesthesia, mice were allowed to recover overnight and then challenged with endotoxin, as previously described (40). Targeted photostimulation of cholinergic neurons in the brainstem DMN significantly attenuated serum TNF levels in mice receiving endotoxin as compared with sham-stimulated controls (Fig. 1*E*). Photostimulation of the DMN using yellow light (593.5nm), which does not activate ChR2, failed to attenuate TNF in ChAT-ChR2-eYFP

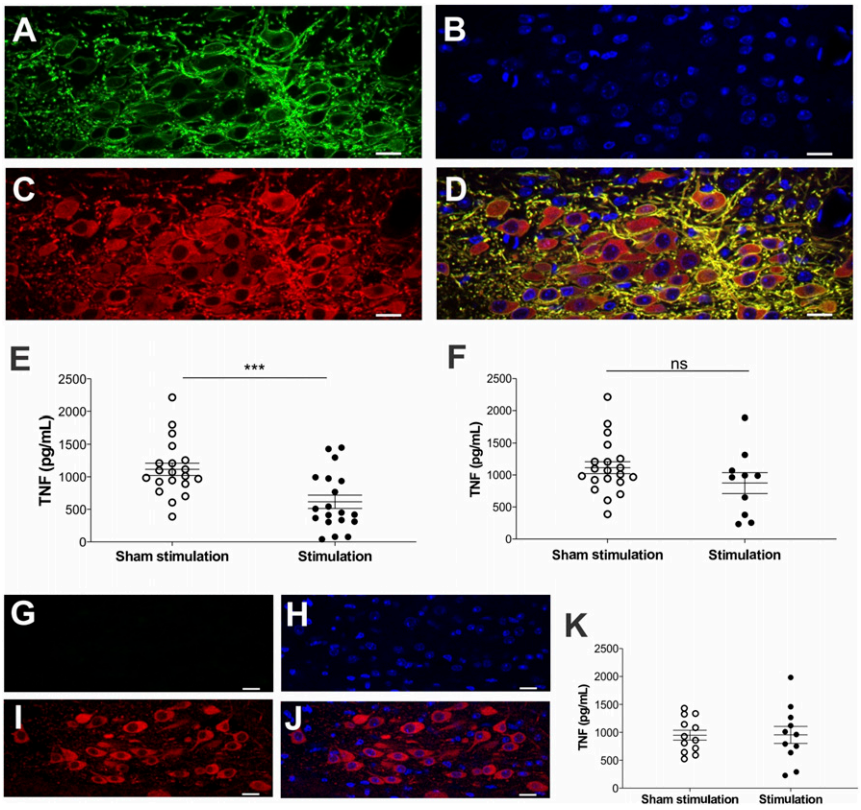

Fig. 1. Selective activation of DMN cholinergic neurons inhibits TNF production during endotoxemia. (*A–D*) Confocal images showing colocalization of ChR2-eYFP and ChAT immunoreactivity in the DMN of ChAT-ChR2-eYFP mice. (*A*) Anti-eYFP staining, (*B*) DAPI, (*C*) anti-ChAT staining, and (*D*) merged image of anti-eYFP, DAPI, and anti-ChAT staining. Note the strong expression of ChR2-eYFP in cholinergic neurons in the DMN. Data are representative of two animals per group. (Scale bar, 20 μm.) 40× magnification. (*E* and *F*) Optogenetic stimulation of cholinergic neurons in the DMN attenuated serum TNF in endotoxemic mice. ChAT-ChR2-eYFP mice were subjected to sham stimulation or optogenetic stimulation using (*E*) blue light (473 nm, 20 Hz, 25% duty cycle, 5 min) or (*F*) yellow light (593.5 nm, 20 Hz, 25% duty cycle, 5 min) in the left DMN. Animals were allowed to recover for 24 h and then injected intraperitoneally with LPS. Serum was obtained 90 min post-LPS administration and TNF was measured by ELISA. Stimulation of ChR2-expressing DMN cholinergic neurons with blue light, but not with yellow light, suppressed TNF levels during endotoxemia in ChAT-ChR2-eYFP mice. Data are represented as individual mouse data points with mean ± SEM. Unpaired *t* test: sham versus optogenetic stimulation (***$P < 0.001$, $n = 19$ to 20 per group). (*G–J*) Confocal images showing the absence of ChR2-eYFP in cholinergic neurons in littermate control mice. (*G*) Anti-eYFP staining, (*H*) DAPI, (*I*) anti-ChAT staining, and (*J*) merged image of anti-eYFP, DAPI, and anti-ChAT staining. Data are representative of two animals per group. (Scale bar, 20 μm.) 40× magnification. (*K*) Optogenetic stimulation in the DMN using blue light (473 nm, 20Hz, 25% duty cycle, 5 min) failed to suppress TNF production in ChR2-eYFP littermate controls. Data are represented as individual mouse data points with mean ± SEM. $n = 11$ to 12 per group.

mice (Fig. 1*F*). Photostimulation of DMN neurons in littermate controls (noncarriers) not expressing ChR2-eYFP (Fig. 1 *G*–*J*) also failed to suppress TNF levels (Fig. 1*K*). Thus, selective activation of brainstem DMN cholinergic neurons inhibits TNF production during endotoxemia.

DMN Cholinergic Fibers Terminate in the Celiac-Superior Mesenteric Ganglion Complex. Efferent vagus nerve–splenic nerve interaction within the celiac-superior mesenteric ganglion complex has been implicated in the inflammatory reflex (17, 19, 21, 24, 41, 42). The celiac-superior mesenteric ganglionic complex receives preganglionic innervations from the thoracic splanchnic nerves. It also receives cholinergic fibers from the vagus nerve. To localize the celiac-superior mesenteric ganglion complex, we used ChAT-enhanced green fluorescent protein (eGFP) transgenic mice, expressing GFP under the control of ChAT promoter, allowing fluorescent visualization of cholinergic neuronal projections. Using fluorescent stereomicroscopy, we localized the celiac-superior mesenteric ganglion complex on the ventral side of the descending aorta, supero-medial to the kidneys (Fig. 2 *A* and *B*) as previously reported in mice (43) and rats (44, 45).

We used an adeno-associated virus (AAV) vector approach to specifically visualize the termination of vagus nerve fibers in the celiac-superior mesenteric ganglion complex. Cre recombinase-sensitive replication-deficient AAV serotype 5 engineered to express both ChR2 and eYFP (AAV5-ChR2-eYFP) was administered into the left DMN of mice expressing Cre recombinase under transcriptional control of synapsin promoter (Syn-cre mice) (Fig. 2*C*). The anterograde property of AAV tracers allows mapping of the axonal projections of efferent vagus fibers originating in the DMN because Cre-expressing efferent vagus neurons transduced by AAV5-ChR2-eYFP express eYFP. Immunohistochemical analysis of the celiac-superior mesenteric ganglion complex revealed eYFP-expressing vagus terminals in mice that received AAV5-ChR2-eYFP in the brainstem DMN nucleus (Fig. 2*D*), indicating that vagus nerve efferent fibers originating in the DMN project to the celiac-superior mesenteric ganglia. In contrast, cell bodies of neurons originating in the celiac-superior mesenteric ganglia stained with DAPI (4′,6-diamidino-2-phenylindole) and the neuronal marker NeuN failed to express eYFP (Fig. 2 *E*–*G*). As AAV5 tracers are not capable of transsynaptic transfer, the presence of eYFP in neuronal terminals confirms previous findings that vagus efferent fibers originating in the DMN innervate the celiac-superior mesenteric ganglia (44, 45). Synaptophysin is an integral membrane glycoprotein of neuronal presynaptic vesicles in synapses and is involved in neurotransmitter exocytosis (46, 47). Immunohistochemistry for eYFP-expressing vagus nerve terminals (Fig. 2*H*) and synaptophysin (Fig. 2*I*) revealed coexpression of eYFP-expressing DMN vagus nerve fibers and synaptophysin in the celiac-superior mesenteric ganglia (Fig. 2*J*). Manders' overlap coefficient analysis (48) of the colocalization image (Fig. 2*K*) showed coexpression of synaptophysin and eYFP with a proportion of 0.25 ± 0.3 (Fig. 2*L*). These data provide direct evidence that efferent vagus nerve fibers originating from the brainstem nucleus DMN terminate in the celiac-superior mesenteric ganglia.

Next, we administered a Cre-dependent replication-deficient herpes virus expressing both channelrhodopsin-2 and fluorescent mCherry proteins (HSV1-ChR2-mCherry) directly into the spleen parenchyma (Fig. 2*C*). Injecting the retrograde herpes virus in the spleen labeled splenic neuron cell bodies in the celiac-superior mesenteric ganglia with fluorescent mCherry protein (Fig. 2 *M* and *N*). Analysis of the celiac-superior mesenteric ganglion complex revealed synaptophysin+ eYFP-expressing efferent vagus nerve terminals projecting from the brainstem DMN forming highly varicose structures around mCherry-expressing splenic nerve cell bodies (Fig. 2*O*). More than 40% of synaptophysin+ eYFP-expressing efferent vagus nerve terminals were in close proximity (≤300 nm) to mCherry-expressing splenic nerve cell bodies in the celiac-superior mesenteric ganglia (Fig. 2*O*). These findings reveal that projections from cholinergic neurons originating in the brainstem DMN terminate in close proximity to splenic nerve cell bodies in the celiac ganglia.

Optogenetic Stimulation of DMN Cholinergic Cell Bodies Induces Evoked Action Potentials in the Splenic Nerve. To determine whether action potentials originating in the cholinergic efferent vagus nerve projecting from the brainstem DMN are transmitted to the splenic nerve, we recorded splenic nerve activity in real time during optogenetic stimulation of the cholinergic neurons in the DMN. A micro cuff recording electrode was implanted on the splenic nerve of ChAT-ChR2-eYFP mice prior to optogenetic stimulation of the brainstem DMN cholinergic neurons. Photostimulation of the DMN cholinergic neurons using blue light (473 nm) significantly increased splenic nerve electrical activity in ChAT-ChR2-eYFP mice, but not in noncarrier controls lacking ChR2 expression (Fig. 3 *A* and *B*). The firing frequency of splenic nerve activity was significantly increased during photostimulation of the DMN in ChAT-ChR2-eYFP mice but not in noncarrier controls (Fig. 3 *C* and *D*). Administration of bupivacaine (49), which targets voltage-gated sodium channels to inhibit depolarization, to the left cervical vagus nerve inhibited splenic nerve activity mediated by DMN optogenetic stimulation (Fig. 3 *E* and *F*). These results provide direct evidence that DMN cholinergic neurons propagate signals via efferent vagus nerve fibers to stimulate splenic nerve activity.

Electrical Stimulation of the Vagus Nerve Induces Efferent Signals to Evoke Action Potentials in the Splenic Nerve. Next, rats were implanted with micro cuff recording electrodes on both the subdiaphragmatic vagus nerve (proximal to the celiac-superior mesenteric ganglia) and the splenic nerve (Fig. 4*A*). A bipolar electrode delivering biphasic, charge-balanced pulses to the cervical vagus nerve-evoked compound action potentials (CAPs) in the subdiaphragmatic vagus nerve and in the splenic nerve (Fig. 4 *B* and *C*). Selective surgical transection of the cervical vagus nerve (vagotomy) caudal to the stimulating electrode prevented evoked compound action potentials in the subdiaphragmatic vagus nerve and splenic nerve (Fig. 4 *D*–*G*). In contrast, vagotomy rostral to the cervical-stimulating electrode failed to prevent recording evoked compound action potentials in the subdiaphragmatic vagus nerve and splenic nerve (Fig. 4 *D*–*G*). To study whether signals originating in the vagus nerve are transmitted via the celiac-superior mesenteric ganglion complex to the splenic nerve, we performed selective splenic neurectomy. Transecting the splenic nerve caudal to the celiac-superior mesenteric ganglia, yet proximal to the splenic nerve recording electrode (Fig. 4*H*), prevented vagus nerve-elicited evoked compound action potentials in the splenic nerve (Fig. 4 *I* and *J*). In contrast, cutting the splenic nerve distal to the splenic nerve recording electrode failed to inhibit splenic nerve-evoked potentials (Fig. 4 *H*–*J*). Together these data indicate efferent vagus nerve signals traverse the celiac-superior mesenteric ganglia to induce evoked action potentials in the splenic nerve.

To examine whether vagus nerve-elicited evoked potentials in the splenic nerve requires ganglionic cholinergic neurotransmission, we recorded the splenic nerve and subdiaphragmatic vagus nerve after administering hexamethonium bromide, which blocks cholinergic ganglionic neurotransmission (50). Administration of hexamethonium bromide abrogated vagus nerve-elicited evoked potentials in the splenic nerve (Fig. 4 *K* and *M*) but not in subdiaphragmatic vagus fibers (Fig. 4*L*), indicating that vagus nerve signals evoke splenic nerve action potentials through cholinergic ganglionic neurotransmission. Electromyography (EMG) of laryngeal muscles innervated by the vagus nerve confirmed that electrical stimulation of the cervical vagus nerve stimulated increased EMG signals (*SI Appendix*, Fig. S2*A*).

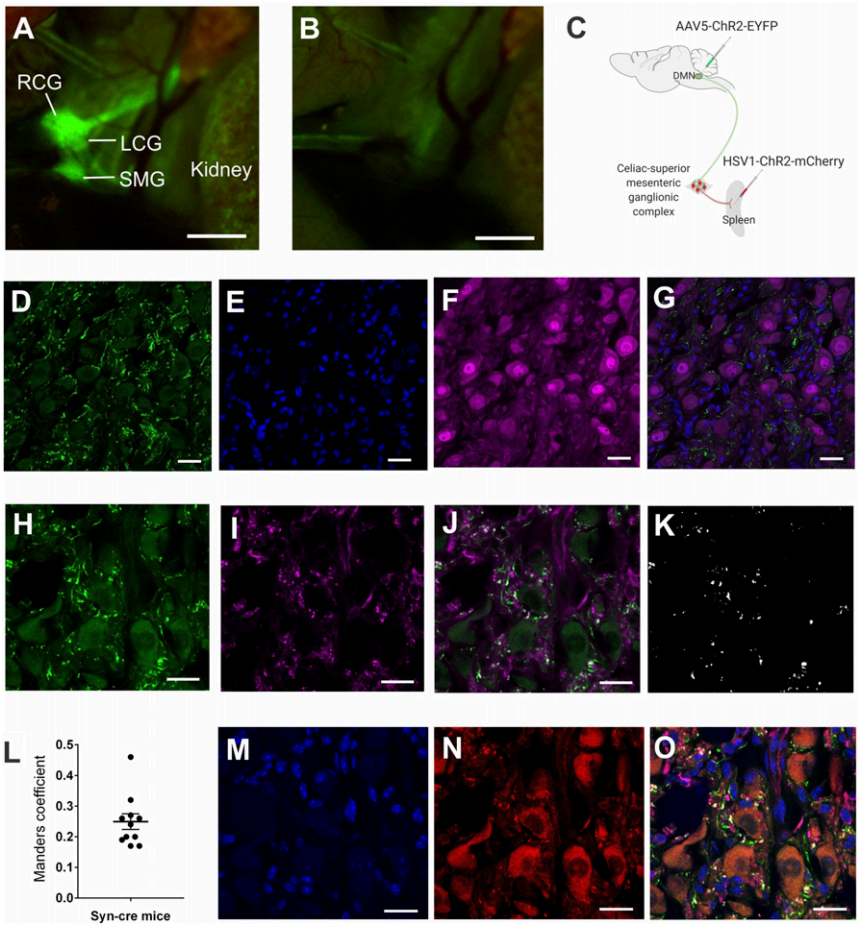

Fig. 2. The efferent vagus nerve fibers terminate in close proximity to the splenic nerve in the celiac-superior mesenteric ganglion complex. (*A*) Identification of the celiac-superior mesenteric ganglion complex in ChAT-eGFP transgenic mice, which allow fluorescent visualization of cholinergic structures. Using fluorescent stereomicroscopy, the celiac-superior mesenteric ganglion complex was localized on the ventral side of the descending aorta, supero-medial to the kidneys. RCG, right celiac ganglion; LCG, left celiac ganglion; SMG, superior mesenteric ganglion. Data are representative of two animals per group. (*B*) Only autofluorescence was seen in control C57BL/6 mice using fluorescent stereomicroscopy on the same area. (*C*) Schematic depiction of the viral tracing strategy, which involved infection of a Cre-dependent AAV (AAV5- ChR2-eYFP) into the DMN and a Cre-dependent HSV (HSV-ChR2-mCherry) into the spleen parenchyma of Syn-Cre mice. (*D–G*) eYFP-expressing efferent vagus terminals and NeuN+ nerve cell bodies were visualized by immunohistochemistry in the celiac-superior mesenteric ganglia. (*D*) anti-eYFP staining, (*E*) DAPI, (*F*) anti-NeuN staining, (*G*) merged image of anti-eYFP, anti-NeuN, and DAPI staining. Note eYFP-expressing efferent vagus terminals in close proximity to NeuN-expressing nerve cell bodies. Data are representative of two animals per group. (Scale bar, 25 μm.) 40× magnification. (*H–L*) Colocalization analysis of synaptophysin and eYFP in presynaptic efferent vagus nerve terminals in the celiac-superior mesenteric ganglion complex. (*H*) Anti-eYFP staining, (*I*) anti-synaptophysin staining, (*J*) merged image of anti-eYFP, and anti-synaptophysin staining. (*K*) Colocalization mask showing overlap regions of eYFP and synaptophysin labeling. (*L*) Mander's coefficient values for overlap proportion. Presynaptic terminals labeled with anti-synaptophysin colocalized with anti-eYFP with a proportion of 0.25 ± 0.3 (Mander's coefficient), indicating that vagus nerve fibers originating from the DMN terminate in the celiac-superior mesenteric ganglion complex. (Scale bar, 20 μm.) 63× magnification. (*M–O*) eYFP-expressing efferent vagus terminals and mCherry-expressing splenic nerve cell bodies were visualized by immunohistochemistry in the celiac-superior mesenteric ganglion complex. (*M*) DAPI, (*N*) mCherry, (*O*) merged image of anti-eYFP, anti-synaptophysin, mCherry and DAPI staining. (Scale bar, 20 μm.) 63× magnification. Note a substantial proportion ($41.3 \pm 3.4\%$) of synaptophysin+ eYFP+ presynaptic vagus terminals are located in close proximity (<300 nm) to splenic neurons retrogradely labeled by HSV-mCherry.

Caudal, but not rostral, vagotomy abolished the EMG responses to vagus nerve stimulation (Fig. 4*D* and *SI Appendix*, Fig. S2*B*). As expected from prior studies (13, 16, 24, 51), cervical vagus and splenic nerve stimulation significantly inhibited TNF production during endotoxemia in rats (Fig. 4*N*) and in mice (*SI Appendix*, Fig. S3). Together these data indicate that efferent vagus nerve signals elicited by either optogenetic stimulation of DMN cholinergic neurons or direct electrical stimulation of the cervical vagus nerve generate evoked responses in the splenic nerve through a mechanism that requires ganglionic neurotransmission via the celiac-superior mesenteric ganglion complex.

First described almost 200 y ago (52), the brainstem nucleus DMN, lying anterior and lateral to the base of the fourth ventricle in the medulla oblongata, occupies a role in maintaining physiological homeostasis, including pulmonary and cardiovascular functions, feeding behavior, and metabolism. The vagus nerve comprises efferent vagus nerve fibers that originate in the DMN and the nucleus ambiguus (44). Our data now show that selective activation of efferent cholinergic vagus nerve fibers originating in the DMN is sufficient to activate the inflammatory reflex and inhibit the production of TNF. Although numerous studies have demonstrated the efficacy of efferent vagus nerve signaling in regulating TNF and other proinflammatory cytokine levels and attenuating the severity of inflammatory syndromes, the origin and functional identity of the vagus nerve fibers of the inflammatory reflex were previously unknown. Unlike electrical vagus nerve stimulation, which may recruit multiple neuronal subtypes, optogenetics enables precise temporal control of specific

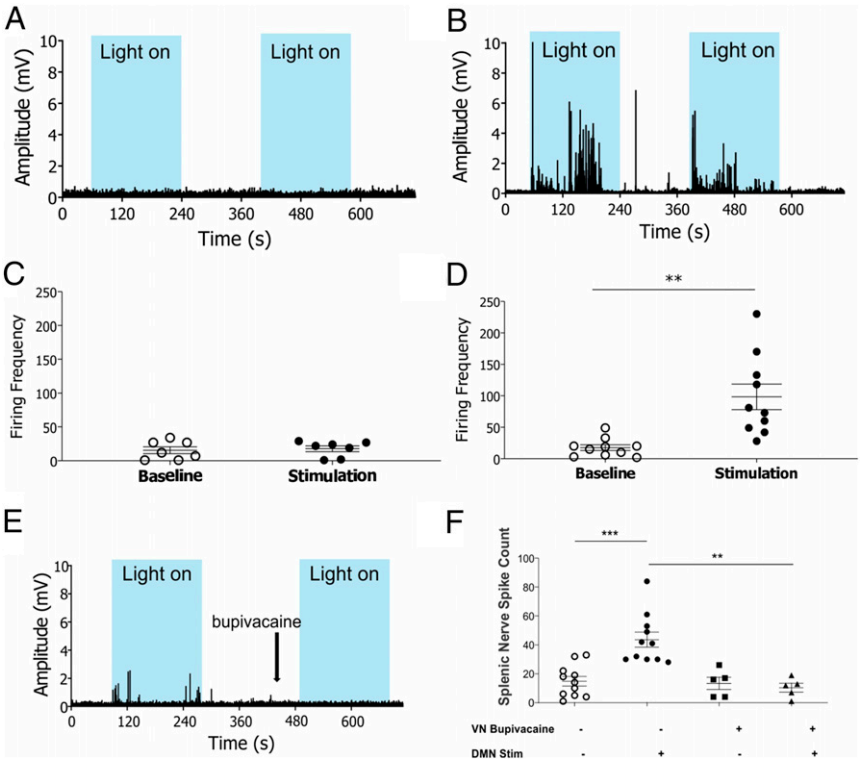

Fig. 3. Optogenetic stimulation of cholinergic neurons in the DMN induces evoked action potentials in the splenic nerve. (*A* and *B*) Splenic nerve activity in response to blue light stimulation (light on) of the DMN cholinergic neurons (473 nm, 25% duty cycle, 8 to 12 mW total power, 2 to 3 min duration). Blue boxes indicate periods of light stimulation. Representative recordings shown for (*A*) non-ChR2 littermate control (*B*) ChAT-ChR2-eYFP mice. Data are representative of 7 to 10 animals per group. (*C* and *D*) Optogenetic stimulation of DMN cholinergic neurons produced a significant increase in splenic nerve activity in ChAT-ChR2-eYFP mice. Firing frequency was recorded in the splenic nerve over a 2-min stimulation period in (*C*) non-ChR2 littermate control, (n = 7), (*D*) ChAT-ChR2-eYFP mice (n = 10). Data are represented as individual mouse data points with mean ± SEM. Two-tailed t test: baseline versus optogenetic stimulation (**$P < 0.01$). (*E* and *F*) Optogenetic stimulation of DMN cholinergic neurons following bupivacaine administration to the left cervical vagus nerve failed to induce evoked potentials in the splenic nerve. (*E*) Splenic nerve activity was recorded during optogenetic stimulation (473 nm, 25% duty cycle, 8 to 12 mW total power, 2 min duration) of the DMN pre- and postbupivacaine administration. Blue boxes indicate periods of light stimulation. Representative neural recording shown. Data are representative of five animals. (*F*) Total spike count measured in splenic nerve following optogenetic stimulation of the DMN. Data are represented as individual mouse data points with mean ± SEM. Two-tailed t test: sham versus DMN stimulation (***$P < 0.001$, n = 11), vehicle versus bupivacaine administration (**$P < 0.01$, n = 5). No significant difference in the baseline splenic nerve activity was observed after the addition of bupivacaine to the left cervical vagus nerve.

neuronal populations in vivo (36). Because selective optogenetic stimulation of DMN cholinergic neurons in ChAT-ChR2-eYFP-expressing mice significantly attenuates TNF responses, we now have direct experimental evidence the DMN neurons control the innate immune system response to inflammation.

The spleen is innervated by adrenergic nerve fibers that originate in the celiac-superior mesenteric ganglion complex (22, 23). We previously demonstrated the spleen is devoid of cholinergic fibers (21), and norepinephrine modulates acetylcholine producing T lymphocytes (21, 24). Using genetically targeted viral tracers, here we show preganglionic efferent vagus nerve fibers originating in the brainstem DMN terminate in the celiac-superior mesenteric ganglia in close proximity to splenic nerve cell bodies. DMN-derived efferent vagus nerve terminals enter the celiac-superior mesenteric ganglia through efferent fibers of its celiac branches and terminate in highly varicose synaptic-like structures around the principle ganglion cells in the celiac-superior mesenteric ganglia (44, 45). Splenic denervation and reserpine-induced depletion of adrenergic nerves abolish the anti-inflammatory effect of cervical vagus nerve stimulation (21). While it is plausible that other brainstem nuclei modulate immunity, our data give genetic and functional evidence of signals originating in the DMN which traverse cholinergic efferent vagus nerve fibers, the celiac-superior mesenteric ganglia, and the splenic nerve to inhibit cytokine production in the spleen.

By combining optogenetics, anatomical and functional mapping, and direct assessment of the immune response, we have identified the DMN as an important locus that regulates immunity. These findings also offer an understanding of neuro-immune communication as a complex interaction between parasympathetic cholinergic neurons and sympathetic adrenergic neurons. This challenges the classical view that the parasympathetic and the sympathetic divisions of the autonomic nervous system always act in opposition.

Materials and Methods

Animals. All procedures with experimental animals were approved by the Institutional Animal Care and Use Committee and the Institutional Biosafety Committee of the Feinstein Institute for Medical Research, Northwell Health, Manhasset, NY in accordance with NIH guidelines. Animals were maintained at 25 °C on a 12-h light-dark cycle with free access to food and water. Male balb/C mice and Sprague-Dawley rats were obtained from Taconic (Taconic Biosciences, Inc.). *ChAT-ChR2-eYFP* BAC (B6.Cg-Tg(Chat-COP4*H134R/eYFP,Slc18a3)6Gfng/J) transgenic mice and *Syn-Cre* (B6.Cg-Tg(Syn1-cre)671Jxm/J) mice were purchased from Jackson Laboratory (Jackson Laboratory) and maintained as hemizygous in fully accredited facilities at the Feinstein Institute for Medical Research. Control mice consisted of *ChAT–ChR2–eYFP* or *Syn-Cre* negative littermates. Only male mice (8 to 12 wk old) and rats (2 to 4 mo old) were used in these studies.

Activation of DMN Cholinergic Neurons Using Optogenetics. ChAT-ChR2-eYFP mice were used for optogenetic experiments. While under anesthesia with a

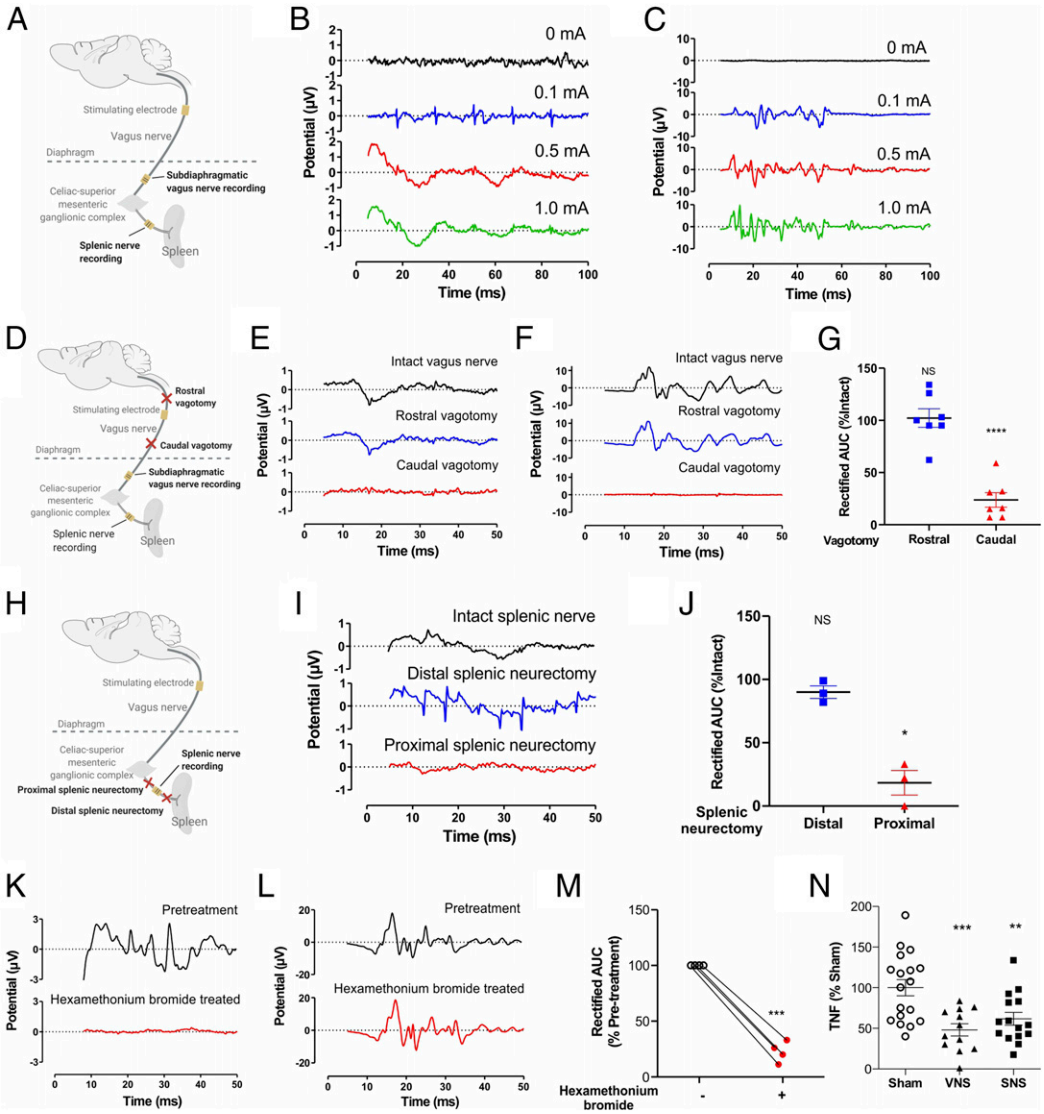

Fig. 4. Efferent cholinergic signals transmitted in the vagus nerve induce evoked action potentials in the splenic nerve. (*A–C*) Evoked splenic nerve compound action potentials increase in response to increasing intensities of electrical cervical vagus nerve stimulation. (*A*) Schematic depiction of the recording strategy. (*B–C*) Stimulation (0.25 ms biphasic pulses of 0, 0.1, 0.5, 1 mA) was delivered to the cervical vagus nerve, and evoked compound action potentials were recorded on the splenic nerve and subdiaphragmatic vagus nerve. Representative traces of (*B*) splenic nerve, (*C*) subdiaphragmatic vagus nerve. Data is representative of 3 animals per group. (*D–G*) Efferent signals transmitted in the cervical vagus nerve induce evoked action potentials in the splenic nerve. (*D*) Schematic depiction of the vagotomy and recording strategy. After caudal or rostral vagotomy (with respect to stimulating electrode), vagus nerve stimulation-induced evoked potentials were recorded. Representative traces of (*E*) splenic nerve, (*F*) subdiaphragmatic vagus nerve. Data is representative of 7 animals per group. (*G*) Caudal but not rostral vagotomy abrogates evoked action potentials in the splenic nerve. Data is represented as individual rat data point with mean ± SEM. One-way paired mixed-effects model followed by Tukey's multiple comparisons test between groups: intact versus caudal vagotomy ($P < 0.0001$, $n = 7$), rostral versus caudal vagotomy ($P = 0.0008$, $n = 7$). (*H–J*) Splenic nerve activity in response to vagus nerve stimulation recorded after splenic neurectomy (proximal or distal to the splenic nerve recording electrode), (*H*) Schematic depiction of the splenic neurectomy and recording strategy. After proximal or distal splenic neurectomy (with respect to recording electrode) vagus nerve stimulation-induced evoked potentials were recorded, (*I*) Representative traces of compound action potentials in the splenic nerve. Data is representative of 3 animals per group, (*J*) Splenic neurectomy that was proximal but not distal to the splenic nerve recording electrode abrogates evoked action potentials in the splenic nerve. Data is represented as individual rat data point with mean ± SEM. Paired mixed-effects model followed by Tukey's multiple comparisons test between groups: intact versus proximal splenic neurectomy ($P = 0.02$, $n = 3$). (*K–M*) Blocking of cholinergic signaling with hexamethonium bromide (10 mg/kg) abrogates cervical vagus nerve-originating evoked potentials in the splenic nerve. Vagus nerve stimulation-induced evoked potentials were recorded in the (*K*) splenic nerve and (*L*) sub-diaphragmatic vagus nerve before injection and at 20 min post-injection. Representative examples of evoked potentials ($n = 4$ per group). (*M*) Area under the curve (AUC) of the splenic nerve activity. Data is represented as individual rat data point with mean ± SEM. Paired t-test between two groups: Pre-treatment versus post-treatment with hexamethonium bromide ($P = 0.0005$, $n = 4$). (*N*) Splenic nerve stimulation attenuates LPS-induced serum TNF response. Data is represented as individual rat data point with mean ± SEM. One-way ANOVA followed by Dunnett's multiple comparisons test between groups: sham versus VNS ($P < 0.001$), sham versus SNS ($P < 0.01$).

mixture of ketamine (144 mg/kg) and xylazine (13 mg/kg), mice were placed in a stereotaxic frame (David Kopf Instruments) and held in place with bilateral ear bars. A midline skin incision was made in the posterior neck and the subcutaneous (s.c.) tissues and paraspinal muscles were retracted laterally, exposing the dura mater. The head was tilted down 45° to lift the cerebellum off the brainstem and to visualize the fourth ventricle. A bent 23G needle was carefully inserted into the dura mater, without injuring the underlying brainstem nor vessels. The base of the fourth ventricle and obex

were identified after clearing the cerebrospinal fluid (CSF). Under stereotaxic guidance, a 200 μm fiber optic cannula (Thorlabs) was inserted into the left DMN (0.25 mm lateral to the obex and 0.48 mm deep to the brainstem surface). In a separate group of mice, DiI dye was injected at this location to mark the DMN. To activate cholinergic neurons by light pulse (frequency: 20 Hz, 25% duty cycle, 5-min duration), a function generator (Agilent) was connected to a blue laser source (Opto Engine LLC). Light intensity was maintained between 7 to 15 mW/mm^2 at the cannula tip. Sham stimulation was carried out the same way with the exception that, following fiber optic cannula insertion, no laser stimulation was performed. Following optogenetic stimulation or sham stimulation, the fiber optic cannula was removed, the wound was approximated in two layers using 5–0 vicryl sutures (Ethicon), and covered with Vetbond tissue adhesive. Mice were allowed to recover on a heat pad, and then returned to the colony room.

Endotoxemia. Mice or rats subjected to either optogenetic stimulation or electrical stimulation were allowed to recover overnight prior to endotoxemia. Lipopolysaccharide (LPS, *Escherichia coli* 0111:B4; Sigma; 1 mg/mL in saline) was sonicated for 30 min and administered intraperitoneally (0.25 mg/kg to mice and 5 mg/kg to rats). Animals were euthanized by CO_2 asphyxiation 90 min post-LPS administration and blood was collected by cardiac puncture. Serum TNF levels were quantitated using commercial enzyme-linked immunosorbent assay (ELISA) (Invitrogen).

Brainstem and Spleen Injections. *Syn-Cre* mice were used for viral injections. Mice were anesthetized with ketamine (144 mg/kg)/xylazine (13 mg/kg), placed in a stereotaxic frame, and the base of the fourth ventricle and obex were identified as described earlier. For AAV5-ChR2-eYFP (pAAV-EF1a-double floxed-hChR2(H134R)-eYFP-WPRE-HGHpA [Addgene 20298]; Penn Vector Core Gene Therapy Program) virus injections, a glass micropipette (FIVEphoton Biochemicals) was inserted into the left DMN of the left hemisphere (AP -7.32; ML – 0.25; DV + 0.48). Virus solution was injected (40 nL) using a Picospritzer III microinjection system (Parker) (20 injections of ∼2 nL each at 3 PSI and 10 ms duration). Following viral injection, the micropipette was removed, the wound was approximated in two layers and covered with Vetbond tissue adhesive.

For HSV injections in the spleen, while still under anesthesia, the spleen was exposed via a midline incision and a separate glass micropipette containing HSV1-ChR2-mCherry (hEF1a-LS1L-hChR2[H134R]-mCherry; Gene Delivery Technology Core. MGH Neurology) was used to inject ∼40 nL virus (20 injections of ∼2 nL each at 3 PSI and 10 ms duration) into the splenic parenchyma. Following injection, the micropipette was removed and the midline incision was closed in two layers with 5–0 vicryl sutures. Mice were allowed to recover for 4 wk and then used for histological analysis of expression of eYFP in vagus terminals and mCherry in splenic nerve cell bodies in the celiac ganglia.

Immunohistochemistry. For ChAT and eYFP staining, ChAT-ChR2-eYFP mice were euthanized with CO_2 asphyxiation and transcardially perfused with chilled phosphate-buffered saline (PBS) followed by chilled 4% paraformaldehyde (PFA). The brain was removed and postfixed in 4% PFA solution at 4 °C overnight. A series of 50 μm free-floating sections were obtained with a vibrotome (Leica VT1200S; Leica Microsystems), and incubated with 0.2% Triton-X 100 for 30 min, followed by blocking solution (10% donkey serum, 0.05% Triton-x 100) for 2 h. After a PBS wash, the sections were incubated with primary antibodies at 4 °C for 3 d. The sections were washed with PBS and then incubated with secondary antibodies for 1 h at room temperature. After another wash in PBS, the sections were mounted using Vectashield anti-fade mounting medium with DAPI (Vector Laboratories). Fluorescence images were acquired on a confocal microscope (Zeiss LSM880; Zeiss) and analyzed using FIJI software. Primary and secondary antibodies were diluted in 2% donkey serum and 0.01% Triton-X 100 as follows: anti-ChAT goat antibody (EMD Millipore) at 1:200; Alexa Fluor 488-conjugated anti-yellow fluorescent protein (YFP)/green fluorescent protein (GFP) rabbit antibody (Invitrogen) at 1:500; and Alexa Fluor 555-conjugated anti-goat immunoglobulin G (IgG) donkey antibody (Thermo Fisher Scientific) at 1:400.

For histologic analysis of celiac-superior mesenteric ganglia, Syn-Cre mice infected with AAV5-ChR2-eYFP in the DMN and HSV1-ChR2-mCherry in the spleen were euthanized 4 wk postinfection with CO_2 asphyxiation and transcardially perfused with chilled PBS followed by chilled 4% PFA. The left celiac ganglion was removed, postfixed for 30 min in 4% PFA, then overnight in 30% sucrose. After embedding in optimal cutting temperature (OCT) compound on dry ice, 16 μm frozen sections were obtained using a cryostat (Microm HM 505N), and incubated with primary antibodies for 48 h at 4 °C. After a wash in PBS, sections were incubated with secondary antibodies for 2 h at room temperature. After another wash in PBS, sections were mounted with DAPI-Fluoromount-G Clear Mounting Media (Southern Biotech). Fluorescence images were acquired on a confocal microscope and analyzed using FIJI software. Primary and secondary antibodies were diluted in PBS containing 0.2% Triton-X 100, and 0.1% normal goat serum as follows: anti-NeuN mouse antibody (EMD Millipore) at 1:500; Alexa Fluor 488 conjugated anti-GFP rabbit antibody (Thermo Fisher) at 1:1,000; anti-synaptophysin mouse antibody (Abcam) at 1:500; and DyLight 650-conjugated anti-mouse goat antibody (Abcam). The degree of colocalization between eYFP and synaptophysin or eYFP and mCherry was calculated based on the integrated density of each signal independently. Manders' coefficient was calculated with ImageJ. Manders' coefficient varies from 0 to 1, corresponding to nonoverlapping images and 100% colocalization between the two images, respectively.

Electrophysiological Recording. In the first set of experiments, evoked compound action potentials in the splenic nerve were recorded in ChAT-ChR2-eYFP mice during optical stimulation of cholinergic fibers in the DMN. After anesthesia was induced, an abdominal incision was made and the splenic neurovascular bundle was exposed. The pancreas and abdominal adipose tissue were dissected away from the splenic neurovascular bundle and a bipolar cuff electrode (CorTec GmbH) was gently placed on the splenic nerve bundle. The ground wire was inserted into mouse soft tissue. The mouse was then placed in a prone position and a fiber optic probe was placed into the DMN under stereotactic guidance as described above. Splenic nerve activity was recorded from the implanted electrode continuously during the on and off cycles of optogenetic stimulation. Data were acquired at 30 kHz using the OmniPlex Neural Data Acquisition System (Plexon Inc.) and analyzed offline using Spike2 analysis software (Cambridge Electronic Design Ltd). For blockade of signals transmitted in the vagus nerve, bupivacaine (Covetrus) was administered onto the vagus nerve during optogenetic stimulation, and splenic nerve activity was measured.

In a second set of experiments, evoked compound action potentials in the splenic nerve were recorded in rats during electrical stimulation of the cervical vagus nerve. Rats were anesthetized with inhaled isoflurane (1.5 to 3%). A midline cervical incision was made, and the left cervical vagus nerve was isolated and placed in a custom-built bipolar cuff electrode (Microprobes) with a silastic coated platinum-iridium cuff electrode secured around the isolated vagus nerve as a stimulating electrode. Next, a midline laparotomy was made and the subdiaphragmatic vagus nerve was isolated from the esophagus and secured within a bipolar cuff electrode (CorTec GmbH). The splenic nerve and artery were traced from the spleen and secured within a bipolar cuff electrode (CorTec GmbH). Needle EMG electrodes were placed within the musculature adjacent to the larynx. Electrical stimulation was delivered to cervical vagus nerve with a biphasic square wave pulse at 1 to 2.7 Hz with pulse width of 0.25 ms/phase generated by a PowerLab 8/35 (AD Instruments) and driven as constant current by an analog stimulus isolator (A-M Systems 2200). Neural potential data were acquired at 20 kHz, high-pass filtered at 30 Hz, and amplified (2,000 x) using the PowerLab 8/35 acquisition system. EMG input was sampled at 20 kHz using the PowerLab 8/35. The data were then averaged 150 to 200 times to increase signal to noise. In some experiments, either the cervical vagus nerve was selectively lesioned proximal or distal to the stimulating electrode or the splenic nerve was selectively lesioned rostral or caudal to the recording electrode. Cholinergic ganglionic blockade was carried out in some rats by intraperitoneal (i.p.) application of 10 mg/kg hexamethonium bromide (Sigma-Aldrich). To quantitate the splenic nerve compound action potentials, the raw potential data were rectified and the area under the curve (AUC) over the latency period of the CAP (10 to 50 ms) was quantified. The AUC from each treatment condition was normalized to the AUC of the intact baseline condition of each individual rat.

Vagus Nerve and Splenic Nerve Stimulation. Mice and rats were anesthetized with intramuscular injection of ketamine (100 mg/kg) and xylazine (10 mg/kg). Cervical vagus nerve was isolated and placed on a custom-built bipolar cuff electrode (Microprobes) as described previously. For splenic nerve stimulation, a lateral laparotomy was made above the spleen and the splenic nerve was suspended on a bipolar hook electrode (Plastics One). In sham-operated animals only an incision was made. Electrical stimulation was delivered to cervical vagus nerve or splenic nerve for 1 min with a biphasic square wave pulse at 0.75 mA intensity, 0.2 ms pulse width at 10 Hz frequency generated by a PowerLab 8/35. Following stimulation, the musculature was sutured and skin closed with wound clips. After overnight recovery, animals were subjected to endotoxemia as described previously.

Statistics. Data were analyzed using Graphpad Prism software using two-tailed unpaired or paired Student's *t* tests or one-way ANOVA or paired mixed-effects model followed with Dunnett's or Tukey's multiple comparisons test, respectively. For all analyses, $P \leq 0.05$ was considered statistically significant.

Data and Material Availability. All data supporting the findings of this study are available within the paper and its supplementary materials. All study data are included in the article and supporting information.

ACKNOWLEDGMENTS. This study was supported by grants from the NIH (National Institute of General Medical Sciences [NIGMS]) 1R01GM132672-01 to S.S.C., NIGMS 1R35GM118182-01 to K.J.T., NIGMS 1R01GM128008-01 to V.A.P. and National Institute of Allergy and Infectious Diseases (NIAID) 1P01AI102852-01A1 to K.J.T. and S.S.C. and by SetPoint Medical to Y.A.L. We thank Donald B. Hoover from the Department of Biomedical Sciences, East Tennessee State University, and Ona Bloom and Dane Thompson from The Feinstein Institutes for Medical Research for helpful discussions. The schematic diagrams in Figs. 2 and 4 were created using Biorender.

1. W. B. Laughton, T. L. Powley, Localization of efferent function in the dorsal motor nucleus of the vagus. *Am. J. Physiol.* **252**, R13–R25 (1987).
2. R. A. Travagli, G. E. Hermann, K. N. Browning, R. C. Rogers, Brainstem circuits regulating gastric function. *Annu. Rev. Physiol.* **68**, 279–305 (2006).
3. E. Ionescu, F. Rohner-Jeanrenaud, H. R. Berthoud, B. Jeanrenaud, Increases in plasma insulin levels in response to electrical stimulation of the dorsal motor nucleus of the vagus nerve. *Endocrinology* **112**, 904–910 (1983).
4. G. S. Geis, R. D. Wurster, Cardiac responses during stimulation of the dorsal motor nucleus and nucleus ambiguus in the cat. *Circ. Res.* **46**, 606–611 (1980).
5. J. P. Montgomery, P. H. Patterson, Behavioral stress and tumor progression. *Anticancer Res.* **26**, 1189–1192 (2006).
6. H.-R. Berthoud, Anatomical demonstration of vagal input to nicotinamide acetamide dinucleotide phosphate diaphorase-positive (nitrergic) neurons in rat fundic stomach. *J. Comp. Neurol.* **358**, 428–439 (1995).
7. H. R. Berthoud, M. Kressel, W. L. Neuhuber, An anterograde tracing study of the vagal innervation of rat liver, portal vein and biliary system. *Anat. Embryol. (Berl).* **186**, 431–442 (1992).
8. H.-R. Berthoud, N. R. Carlson, T. L. Powley, Topography of efferent vagal innervation of the rat gastrointestinal tract. *Am. J. Physiol.* **260**, R200–R207 (1991).
9. C. A. Dinarello, The proinflammatory cytokines interleukin-1 and tumor necrosis factor and treatment of the septic shock syndrome. *J. Infect. Dis.* **163**, 1177–1184 (1991).
10. K. J. Tracey *et al*., Anti-cachectin/TNF monoclonal antibodies prevent septic shock during lethal bacteraemia. *Nature* **330**, 662–664 (1987).
11. K. J. Tracey *et al*., Shock and tissue injury induced by recombinant human cachectin. *Science* **234**, 470–474 (1986).
12. K. J. Tracey *et al*., Cachectin/tumor necrosis factor induces cachexia, anemia, and inflammation. *J. Exp. Med.* **167**, 1211–1227 (1988).
13. L. V. Borovikova *et al*., Vagus nerve stimulation attenuates the systemic inflammatory response to endotoxin. *Nature* **405**, 458–462 (2000).
14. K. J. Tracey, The inflammatory reflex. *Nature* **420**, 853–859 (2002).
15. H. Wang *et al*., Cholinergic agonists inhibit HMGB1 release and improve survival in experimental sepsis. *Nat. Med.* **10**, 1216–1221 (2004).
16. W. J. de Jonge *et al*., Stimulation of the vagus nerve attenuates macrophage activation by activating the Jak2-STAT3 signaling pathway. *Nat. Immunol.* **6**, 844–851 (2005).
17. S. S. Chavan, V. A. Pavlov, K. J. Tracey, Mechanisms and therapeutic relevance of neuro-immune communication. *Immunity* **46**, 927–942 (2017).
18. S. S. Chavan, K. J. Tracey, Essential neuroscience in immunology. *J. Immunol.* **198**, 3389–3397 (2017).
19. V. A. Pavlov, S. S. Chavan, K. J. Tracey, Molecular and functional neuroscience in immunity. *Annu. Rev. Immunol.* **36**, 783–812 (2018).
20. S. S. Chavan, P. Ma, I. M. Chiu, Neuro-immune interactions in inflammation and host defense: Implications for transplantation. *Am. J. Transplant.* **18**, 556–563 (2018).
21. M. Rosas-Ballina *et al*., Splenic nerve is required for cholinergic antiinflammatory pathway control of TNF in endotoxemia. *Proc. Natl. Acad. Sci. U.S.A.* **105**, 11008–11013 (2008).
22. D. M. Nance, J. Burns, Innervation of the spleen in the rat: Evidence for absence of afferent innervation. *Brain Behav. Immun.* **3**, 281–290 (1989).
23. D. L. Bellinger, S. Y. Felten, D. Lorton, D. L. Felten, Origin of noradrenergic innervation of the spleen in rats. *Brain Behav. Immun.* **3**, 291–311 (1989).
24. M. Rosas-Ballina *et al*., Acetylcholine-synthesizing T cells relay neural signals in a vagus nerve circuit. *Science* **334**, 98–101 (2011).
25. H. Wang *et al*., Nicotinic acetylcholine receptor alpha7 subunit is an essential regulator of inflammation. *Nature* **421**, 384–388 (2003).
26. S. Guarini *et al*., Efferent vagal fibre stimulation blunts nuclear factor-kappaB activation and protects against hypovolemic hemorrhagic shock. *Circulation* **107**, 1189–1194 (2003).
27. B. Lu *et al*., α7 nicotinic acetylcholine receptor signaling inhibits inflammasome activation by preventing mitochondrial DNA release. *Mol. Med.* **20**, 350–358 (2014).
28. T. R. Bernik *et al*., Cholinergic antiinflammatory pathway inhibition of tumor necrosis factor during ischemia reperfusion. *J. Vasc. Surg.* **36**, 1231–1236 (2002).
29. L. V. Borovikova *et al*., Role of vagus nerve signaling in CNI-1493-mediated suppression of acute inflammation. *Auton. Neurosci.* **85**, 141–147 (2000).
30. J. M. Huston *et al*., Splenectomy inactivates the cholinergic antiinflammatory pathway during lethal endotoxemia and polymicrobial sepsis. *J. Exp. Med.* **203**, 1623–1628 (2006).
31. Y. A. Levine *et al*., Neurostimulation of the cholinergic anti-inflammatory pathway ameliorates disease in rat collagen-induced arthritis. *PLoS One* **9**, e104530 (2014).
32. P. S. Olofsson *et al*., α7 nicotinic acetylcholine receptor (α7nAChR) expression in bone marrow-derived non-T cells is required for the inflammatory reflex. *Mol. Med.* **18**, 539–543 (2012).
33. F. A. Koopman *et al*., Vagus nerve stimulation inhibits cytokine production and attenuates disease severity in rheumatoid arthritis. *Proc. Natl. Acad. Sci. U.S.A.* **113**, 8284–8289 (2016).
34. B. Bonaz *et al*., Chronic vagus nerve stimulation in Crohn's disease: A 6-month follow-up pilot study. *Neurogastroenterol. Motil.* **28**, 948–953 (2016).
35. M. C. Genovese *et al*., Safety and efficacy of neurostimulation with a miniaturised vagus nerve stimulation device in patients with multidrug-refractory rheumatoid arthritis: A two-stage multicentre, randomised pilot study. *Lancet Rheumatol.* **2**, E527–E538 (2020).
36. E. S. Boyden, F. Zhang, E. Bamberg, G. Nagel, K. Deisseroth, Millisecond-timescale, genetically targeted optical control of neural activity. *Nat. Neurosci.* **8**, 1263–1268 (2005).
37. D. Wu, L. B. Hersh, Choline acetyltransferase: Celebrating its fiftieth year. *J. Neurochem.* **62**, 1653–1663 (1994).
38. Y. Oda, Choline acetyltransferase: The structure, distribution and pathologic changes in the central nervous system. *Pathol. Int.* **49**, 921–937 (1999).
39. F. Eckenstein, H. Thoenen, Production of specific antisera and monoclonal antibodies to choline acetyltransferase: Characterization and use for identification of cholinergic neurons. *EMBO J.* **1**, 363–368 (1982).
40. L. Tarnawski *et al*., Adenylyl cyclase 6 mediates inhibition of TNF in the inflammatory reflex. *Front. Immunol.* **9**, 2648 (2018).
41. S. P. Bhavnani *et al*.; ASEF-VALUES Investigators, A randomized trial of pocket-echocardiography integrated mobile Health device assessments in modern structural heart disease clinics. *JACC Cardiovasc. Imaging* **11**, 546–557 (2018).
42. K. Murray, M. Barboza, K. M. Rude, I. Brust-Mascher, C. Reardon, Functional circuitry of neuro-immune communication in the mesenteric lymph node and spleen. *Brain Behav. Immun.* **82**, 214–223 (2019).
43. A. M. Downs, C. E. Bond, D. B. Hoover, Localization of α7 nicotinic acetylcholine receptor mRNA and protein within the cholinergic anti-inflammatory pathway. *Neuroscience* **266**, 178–185 (2014).
44. H. R. Berthoud, T. L. Powley, Characterization of vagal innervation to the rat celiac, suprarenal and mesenteric ganglia. *J. Auton. Nerv. Syst.* **42**, 153–169 (1993).
45. H. R. Berthoud, T. L. Powley, Interaction between parasympathetic and sympathetic nerves in prevertebral ganglia: Morphological evidence for vagal efferent innervation of ganglion cells in the rat. *Microsc. Res. Tech.* **35**, 80–86 (1996).
46. B. Wiedenmann, W. W. Franke, Identification and localization of synaptophysin, an integral membrane glycoprotein of Mr 38,000 characteristic of presynaptic vesicles. *Cell* **41**, 1017–1028 (1985).
47. P. Greengard, F. Valtorta, A. J. Czernik, F. Benfenati, Synaptic vesicle phosphoproteins and regulation of synaptic function. *Science* **259**, 780–785 (1993).
48. E. M. M. Manders, F. J. Verbeek, J. A. Aten, Measurement of co-localization of objects in dual-colour confocal images. *J. Microsc.* **169**, 375–382 (1993).
49. A. Scholz, Mechanisms of (local) anaesthetics on voltage-gated sodium and other ion channels. *Br. J. Anaesth.* **89**, 52–61 (2002).
50. J. J. Galligan, J. B. Furness, M. Costa, Effects of cholinergic blockade, adrenergic blockade and sympathetic denervation on gastrointestinal myoelectric activity in Guinea pig. *J. Pharmacol. Exp. Ther.* **238**, 1114–1125 (1986).
51. J. M. Huston *et al*., Splenectomy protects against sepsis lethality and reduces serum HMGB1 levels. *J. Immunol.* **181**, 3535–3539 (2008).
52. B. Stilling, *Ueber die Textur der Medulla oblongata* (Erlangen F Enke, 1843).